THE JOURNAL OF PHYSICAL CHEMISTRY C

pubs.acs.org/JPCC Article

Stress Field Characteristics and Collective Mechanical Properties of Defective Graphene

Bowen Zheng and Grace X. Gu*

Cite This: https://dx.doi.org/10.1021/acs.jpcc.9b11027 Read Online

ABSTRACT: As defects play a pivotal role in the mechanical properties of graphene, much research has been underway to understand their specific effects. However, the determination of mechanical properties of defective graphene such as strength and ductility remains challenging, due to the indeterminacy of local stress distributions, potentially released out-of-plane behavior, and multidefect interactions that are involved when subject to external loads. To cast light on the above complexities, in this paper, stress field characteristics of defective graphene are studied via molecular dynamics simulations, which are shown to be strongly dependent on defect geometries. To detail this influence, defect geometries are decoupled into defect size and shape, where the former determines the area shielded from increasing stress and consequently produces low-stress regions, while the latter determines local stress concentration and governs stress distribution along the defect rim. Additionally, it is shown that the nonuniformity of the stress field can potentially release the out-of-plane degree of freedom and therefore induce spatial patterns. To understand the effects of multiple defects in graphene sheets, an analytical strategy of defect grouping is proposed. The obtained understanding of the defect-affected stress distribution is utilized to rationally optimize the collective mechanical properties of defective graphene sheets. We show that even though the mechanical properties of defective graphene sheets vary with different defect geometry, the proportionality of ultimate strength and failure strain is in general preserved. Finally, the relative significance of the system parameters is discussed. This paper systematically discusses the influence of defects on the stress field and collective mechanical properties of graphene, which solidifies the defect-engineering based tuning approach of the mechanics of graphene as well as other two-dimensional materials.

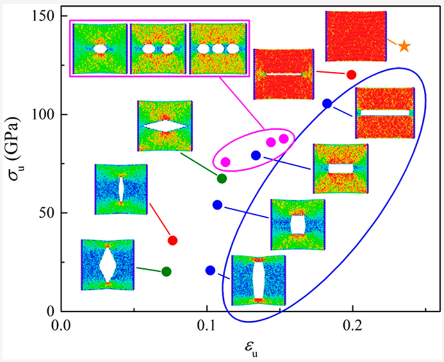

1. INTRODUCTION

Among many celebrated qualities of graphene, the intrinsic mechanical properties of the two-dimensional (2D) material have received tremendous attention and have stimulated research and engineering applications of a broad variety. Despite being one atom thick, the graphene monolayer possesses extraordinary mechanical properties such as an ultrahigh Young's modulus of ~1 TPa[1] and an unsurpassed intrinsic tensile strength of 130 GPa.[1] These mechanical properties make graphene not only ideal for functional composite materials,[2−7] but also an elite base material for nanodevices such as micro/nanoelectromechanical systems (M-/N-EMS),[8,9] supercapacitors,[10,11] transistors,[12,13] spin filters,[14] among others.

Many of the superlative mechanical properties of graphene rely on the nearly perfect periodicity of the 2D scaffold where carbon atoms are placed. Nevertheless, it is not uncommon that a variety of structural defects such as point defects, dislocations, and grain boundaries can be introduced by large-scale synthesis methods such as mechanical exfoliation,[15,16] chemical vapor deposition (CVD),[17,18] and epitaxial growth,[19,20] which may break the perfect periodicity and degrade the mechanical properties of graphene to a great extent. Apart from the above native defects which are dictated by thermodynamics, (patterned) defects can also be deliberately introduced to graphene, which falls into the category of defect engineering.[21−23] By rationally engineering defects the performances of many graphene-based nanodevices have been substantially enhanced. For instance, the creation of Co/N/O tridoped graphene mesh can generate dispersed Co-Nx-C active sites, which can be used to improve the energy efficiency and cycling durability of flexible batteries and wearable electronics.[24] The thermal conductivity of graphene can be improved with oxygen plasma-induced defects, which elevates the performances of graphene-based thermoelectric nanodevices.[25] Graphene kirigami,[26] a defect engineering strategy of graphene inspired by the art of paper cutting, has shown great potential in tuning the mechanical[26,27] and thermal[28] properties of graphene. The shaped graphene monolayer can be stretched up to a strain of 240%,[26] which drastically deviates

Received: November 25, 2019
Revised: March 3, 2020
Published: March 16, 2020

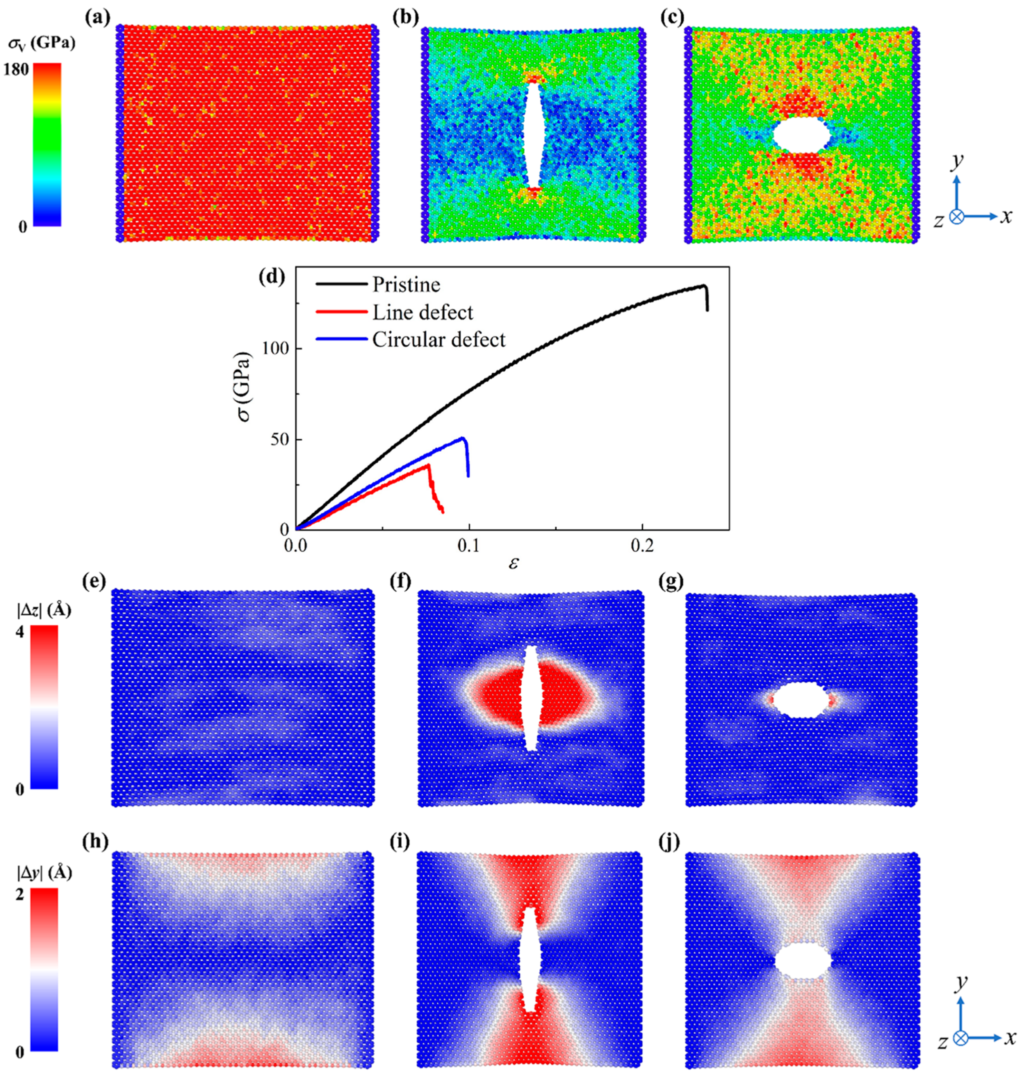

Figure 1. Stress fields, stress−strain curves, and distributions of displacement magnitude of pristine and defective graphene sheets. (a−c) Stress fields, (d) stress−strain curves, and distributions of (e−g) out-of-plane and (h−j) in-plane displacement magnitude of stretched pristine graphene, defective graphene with a line defect, and defective graphene with a circular defect, respectively. Distributions are plotted based on the morphologies right before the initiation of failure.

from the brittle nature of graphene and contributes to an enhanced impact resistance. In the meantime, an ultralow thermal conductivity can be achieved by the design of graphene kirigami, making the graphene family a potential material for thermal management.[28] We have shown in our previous study that, by introducing patterned defects, the mechanical anisotropy of graphene can be fine-tuned. Similar concepts such as graphene nanomesh[29−31] have also exhibited the potential to fine-tune mechanical properties such as enhanced ductility. Therefore, a good understanding of the mechanics of defective graphene not only facilitates the full use of the remarkable mechanical properties but also contributes to the achievement of non-native functionalities.

In recent years, plenty of research has been devoted to the influence of defects on the mechanical properties of graphene and fruitful progress has been made. Hao et al. studied the effect of monatomic vacancies and Stone−Wales dislocations in graphene, showing that the Young's modulus of the graphene sheet has a rather gentle dependence on the defect concentration.[32] Wang et al. studied the effect of defects on the fracture strength of graphene, showing that defects can cause significant strength loss in graphene and the degradation is dependent on temperature and loading conditions.[33] Additionally, the possibility that the defect-induced mechanical degradation of graphene can be recovered by counterintuitively enlarging the defect has been shown.[34] The influences of a defect in other trending 2D nanosheets such as hybrid graphene-boron nitride sheets have also been studied, spinning the tunability of mechanical properties to a broader class of 2D materials.[35,36] Nevertheless, the determination of mechanical properties of defective graphene such as strength and ductility directly based on defect properties remains challenging to date due to the indeterminacy of local stress concentrations and potential out-of-plane behavior when subjected to external loads. As is anticipated, a nonuniform stress field can potentially weaken the structure and lead to early failure, whereas predicting the degree of mechanical degradation directly based on defect information is a nontrivial task. When multiple defects are present, it is even more complex to predict mechanical properties because of potential defect interactions. Hence, it is critical to shed light on the fundamental mechanism and establish a systematic framework on how the

https://dx.doi.org/10.1021/acs.jpcc.9b11027
J. Phys. Chem. C XXXX, XXX, XXX−XXX

existence of defects impact the stress field and the collective mechanical properties of graphene.

In the present paper, stress field characteristics of defective graphene sheets subject to the unidirectional in-plane stretch are studied via molecular dynamics (MD) simulation. Stress fields of various defective graphene sheets are calculated to draw the connection between defect properties and stress distribution, and ultimately to predict collective mechanical properties such as strength and ductility. The altered out-of-plane and in-plane behavior of defective graphene sheets are also inspected and related to stress distribution characteristics. To detail the influence of defect on the stress field, the role of defects is decoupled by separately studying the effects of size and shape. With the knowledge of the fundamental relation between defect properties and stress distribution, the stress field characteristics of graphene sheets with multiple defects are discussed. An application of stress field optimization via rational defect design is presented. This work systematically discusses the influence of defects on the stress distribution in graphene sheets, which opens up the tuning approach of the mechanical properties of graphene as well as other 2D materials via defect design.

2. RESULTS

In this study, square-shaped graphene sheets with a side length of $L \sim 110$ Å are simulated, consisting of 4966 atoms when no defect is present. To achieve various defect designs in graphene sheets, atoms associated with defective regions in graphene are deleted. The unidirectional in-plane stretch is applied in the zigzag direction based on a deformation-control manner by assigning displacement at a constant speed to a 3 Å wide stripe at one end, while a 3 Å-wide stripe at the other end is held immobile in all three dimensions. We want to make a note here that only loading in zigzag direction is studied in the present work, because our previous research has pointed to no qualitative difference between the mechanical properties of zigzag and armchair directions.[34,37] The applied strain rate is constant at 10^9 s^{-1} in all simulations, and the influence of strain rate on the mechanical response of graphene sheets is discussed in more detail in the Supporting Information. More information on system configurations and loading conditions can be found in ref 37. To demonstrate how the existence of defects impacts the mechanical properties, stress fields of graphene sheets are computed which not only can shed light on detailed mechanical responses in an atomic resolution but also can be used to derive collective mechanical properties of the entire graphene sheet.

To begin with, mechanical responses of two defective graphene sheets are studied and compared against pristine graphene. They are (1) a graphene sheet with a centered line defect with a length of 0.5L transverse to the stretch and (2) a graphene sheet with a centered circular defect with a diameter of 0.2L. Stress fields are calculated based on von Mises stress σ_V, of which the details of the calculation methods are provided in the Supporting Information. Stress fields right before the fracture of a pristine graphene and the two defective graphene sheets above are visualized in Figure 1a−c. For the pristine graphene in Figure 1a, stress is uniformly distributed over the whole graphene sheet. Almost every point on the graphene sheet is able to reach a high stress level before failure, suggesting a highly efficient usage of the graphene sheet as a mechanical member where almost all atoms and bonds are leveraged and contribute to the collective mechanical properties. For the defective graphene sheet with a line defect transverse to the stretch, a nonuniform stress field is produced, as is shown in Figure 1b. Upon the stretch the line defect swells laterally and two defect tips localize high stress. In the meantime, along the line defect very low stress is hosted and the low-stress regions propagate in the stretching direction far to the edges of the graphene sheet. It is envisioned that these low-stress regions have little contribution to the collective mechanical properties because the atoms and bonds within are unstressed. In addition, a fracture initiates as soon as the stress of one part of the graphene sheet reaches the bond-breaking stress, which immediately develops causing a catastrophic failure. Because the bond-breaking stress in a defective graphene sheet is no higher than the pristine counterpart, the ultimate stress and strain should be significantly lower than those of the pristine graphene. Next, a graphene sheet with a circular defect is examined to see how the stress field varies with different defect properties, of which the resultant stress field is shown in Figure 1c. Although an uneven stress distribution is also observed, high stress is hosted over a larger area in comparison to the case of a line defect, while regions with a low stress level are significantly smaller, altogether indicating a more uniform stress field. Unlike the case of the line defect where low-stress regions develop in a spread-out manner and propagate to the graphene edges, here low-stress regions grow inwardly and diminish before propagating to the graphene edges. The above stress field properties indicate a better usage of atoms and bonds in comparison to the graphene sheet with a line defect, and thus, the collective mechanical properties should be superior, but still, much lower than the pristine graphene.

To validate the above reasoning on the relation between stress field characteristics and collective mechanical properties, stress−strain curves of the above three graphene sheets are plotted in Figure 1d. The calculation methods of the collective stress σ from MD simulations are provided in the Supporting Information. As is shown, the ultimate stress and strain of the pristine graphene are significantly higher than the two defective graphene sheets, while those of the graphene sheet with a circular defect are higher than one with a line defect. The results of the collective stress−strain relation plus stress fields of the demonstrative examples lead to the following two preliminary conclusions: (1) Various defects can pose different influences on the stress field. (2) The more uniformly stress is distributed upon the stretch, the higher the ultimate stress and strain can reach.

In addition to the ability of defects to alter stress fields, it is interesting to examine whether the existence of defects can induce certain displacement patterns and, if so, how these patterns and the stress field are related. In the literature, outstanding out-of-plane behavior has been observed in designs of graphene kirigami.[26,27,38] However, it remains not well understood how their out-of-plane patterns are related to the stress distribution. Also, the in-plane displacement has not been sufficiently discussed, which may potentially lead to a nontraditional Poisson effect. In this work, we focus on the potential out-of-plane and in-plane behaviors of defective graphene sheets and their relations to the stress field when subject to a unidirectional in-plane stretch.

The displacement in graphene is quantified as follows. For the graphene configurations in this work, the zigzag and armchair directions lie along x and y directions, respectively. Thus, the in-plane stretch is applied in the x direction in the

https://dx.doi.org/10.1021/acs.jpcc.9b11027
J. Phys. Chem. C XXXX, XXX, XXX−XXX

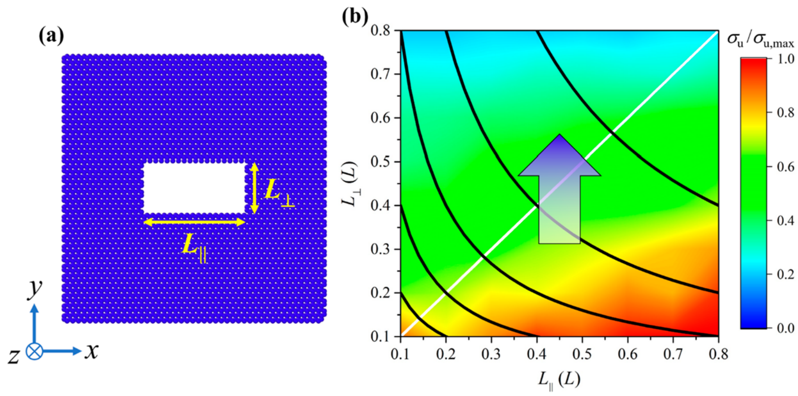

Figure 2. Ultimate strengths of graphene sheets centered a rectangular defect with varying geometric parameter pair $(L_\parallel,L_\perp)$. (a) Illustration of the geometric parameter pair $(L_\parallel,L_\perp)$. (b) Ultimate strength σ_u as a function of $(L_\parallel,L_\perp)$, normalized by $\sigma_{u,max}$ = 107.1 GPa at $(L_\parallel,L_\perp)$ = (0.8L,0.1L). Black lines represent defect geometries sharing the same area. The white line represents square-shaped defects. The arrow indicates the major degradation direction.

$x-y$ plane. We denote the position vector of an atom at time t as $(x(t), y(t), z(t))$. The out-of-plane and in-plane displacement magnitude are expressed as $|\Delta z| = |z(t) - z(0)|$ and $|\Delta y| = |y(t) - y(0)|$. The displacement in the stretching direction $|\Delta x|$ mostly develops with the loading and is therefore not discussed here. The distributions of out-of-plane and in-plane displacement magnitude before fracture of the above three graphene sheets are provided in Figure 1e−g and h−j. For the pristine graphene in Figure 1e, h, the out-of-plane displacement is negligible over the whole domain while a moderate amount of in-plane displacement is exhibited along two free graphene edges, suggesting that the pristine graphene subject to an in-plane stretch can be characterized by totally in-plane lengthening and lateral contraction and is not featured by out-of-plane behavior. For the graphene with a line defect in Figure 1f, i, however, substantial out-of-plane displacement is induced along the defect. Regions with out-of-plane displacement develop inwardly and diminish before reaching the edges of the graphene sheet. Propagation outwardly or parallel to the stretch can violate the zero out-of-plane displacement boundary conditions. In addition, the in-plane displacement is intensified and localized, which develops from the defect and propagates up to the free edges of the graphene sheet. The propagation of regions with in-plane displacement starts from relevant segments of the defect rim and ends at unconstrained edges, exhibiting a spread-out pattern. Viewing segments of the defect rim as the sources of regions with out-of-plane and in-plane displacement, these segments complement each other. For the graphene sheet with a circular defect, although out-of-plane and in-plane displacement are also developed in a similar pattern as the line defect, it is less profound in comparison, as is shown in Figure 1g, j. Only the vicinities of two ends of the circular defect allow for out-of-plane displacement, and the in-plane displacement exhibit a lower magnitude. From the results of defective graphene sheets, it can be concluded that the existence of defects not only renders an out-of-plane degree of freedom which is absent in the pristine graphene, but also intensifies and localizes in-place displacement. Additionally, the displacement features are co-determined by the defect geometry and boundary conditions. Comparing the above distributions of stress and displacement in pristine and defective graphene sheets, the relation between stress field characteristics and out-of-plane and in-plane behavior can be formulated as follows. Out-of-plane displacement can be induced only if the region is featured by low stress. This is because high in-plane stress from stretching will eliminate any out-of-plane tendency due to the equilibrium requirement. High in-plane stress deforms the graphene and gives rise to in-plane displacement. Regions featured by out-of-plane and in-plane displacement are complementary in a way that regions with high stress and low stress are. Hence, it can be concluded that patterned out-of-plane and in-plane displacement is the consequence of defect-induced nonuniform stress field.

The illustrations above have demonstrated the ability of defects to alter the stress distribution and to induce displacement patterns. To cast light on the core factor governing the phenomenon, the effect of defect geometry is studied. The defect geometry can be elucidated by separately discussing the effects of pure size and shape. First, the effect of pure size is investigated. To this end, rectangular defects of various sizes are studied, aiming to minimize the effect of different defect shapes. The total lengths of the projection of defect on the direction parallel and perpendicular to the stretching direction are denoted as $L_\parallel$ and $L_\perp$, respectively. For a rectangular defect with sides parallel and perpendicular to the stretch, two side lengths are exactly $L_\parallel$ and $L_\perp$, as is illustrated in Figure 2a. The effect of defect size $(L_\parallel,L_\perp)$ on the ultimate strength σ_u can be obtained by MD simulations and visualized on an $L_\parallel-L_\perp$ 2D map, as is shown in Figure 2b. The major direction of mechanical degradation is in the positive direction of the $L_\perp$-axis (noted by the arrow), while $L_\parallel$ has a relatively minor influence on the ultimate strength when $L_\perp \gtrsim 0.3L$. It is noteworthy that when $L_\perp < 0.3L$, ultimate stress is enhanced with larger $L_\parallel$, which may be counterintuitive considering the defective graphene sheet is strengthened by enlarging the defect. This is because lengthening the defect along the loading direction elevates the evenness of stress distribution, ultimately leading to improved mechanical properties. However, this phenomenon is in effect only when the length transverse to the loading is small, as is deliberated in ref 34.

On each black line in Figure 2b where defects share the same area, smaller $L_\perp$ indicates superior mechanical properties. The strengthening effect under small $L_\perp$ even adds to the dominancy of the $L_\perp$ effect. To illustrate, the distributions of stress, out-of-plane and in-plane displacement magnitude, and stress−strain curves of four rectangular defects sharing the same area, *i.e.*, (0.1L, 0.8L), (0.2L, 0.4L), (0.4L, 0.2L), and (0.8L, 0.1L), are provided in Figure 3. For graphene sheets

https://dx.doi.org/10.1021/acs.jpcc.9b11027
J. Phys. Chem. C XXXX, XXX, XXX−XXX

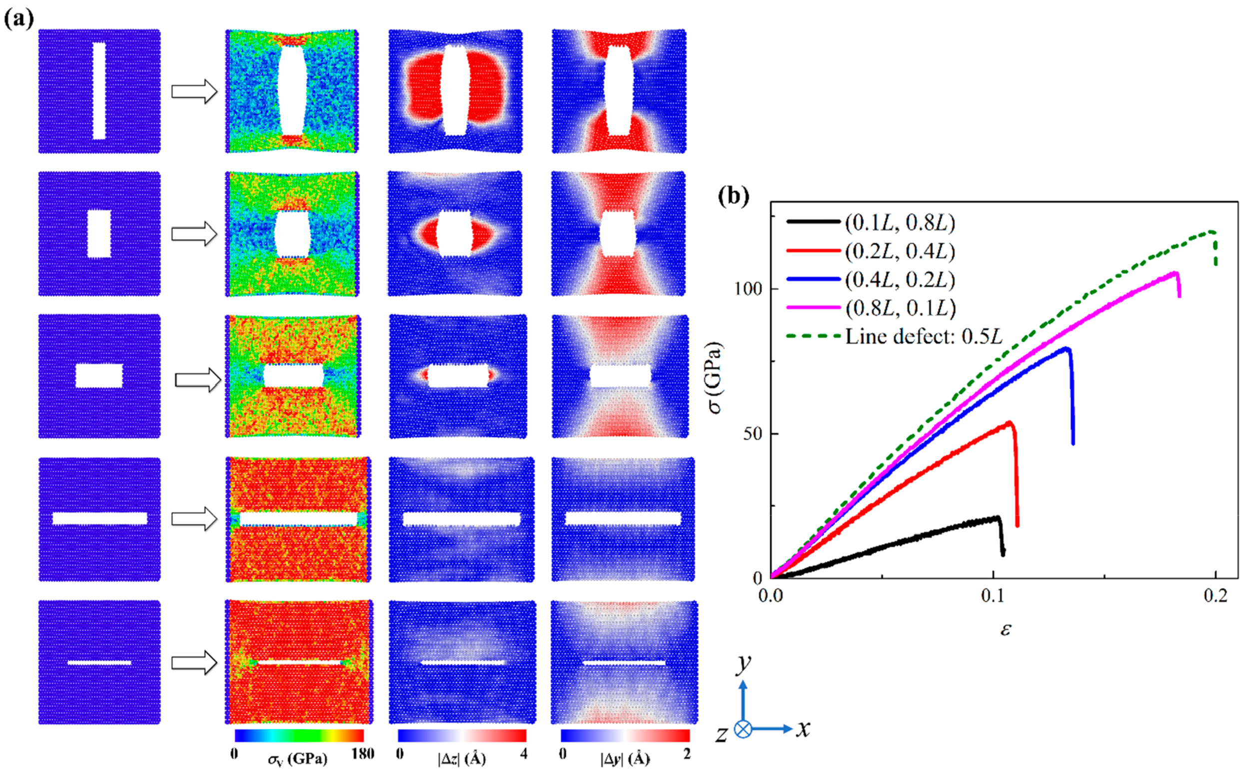

Figure 3. Simulation results of defective graphene sheets with rectangular defects of various $L_{\|}/L_{\perp}$ but a fixed area. (a) Stress fields and distributions of out-of-plane and in-plane displacement magnitude and (b) stress−strain curves of the defective graphene sheets with $(0.1L, 0.8L)$, $(0.2L, 0.4L)$, $(0.4L, 0.2L)$, $(0.8L, 0.1L)$, rectangular defects, and a line defect parallel to the stretch with a length of $0.5L$.

with these rectangular defects, high stress and low stress develop from edges parallel and perpendicular to the stretch, respectively. The covered area of high-/low-stress regions is in general proportional to the length of the corresponding edges. As $L_{\|}$ increases, the stress distribution becomes more and more even. For example, when the size of the rectangular defect transits from $(0.8L, 0.1L)$ to $(0.1L, 0.8L)$, low-stress regions diminish and the high-stress regions expand. It is also notable that high- and low-stress regions are dichotomized at the vertices of the rectangle. When the rectangular defect is reduced down to a line defect parallel to the stretch, stress distributed uniformly over almost the whole graphene sheet except at the immediate vicinities of the two defect tips. A similar tendency applies for the distribution displacement magnitude: as the ratio $L_{\|}/L_{\perp}$ increases, regions exhibiting out-of-plane displacement shrink while regions exhibiting in-plane displacement expand in area but are reduced in intensity; when the rectangle degenerates to a line, both displacement features resemble those of a pristine graphene. Stress−strain curves of above defective graphene sheets with a rectangular defect as well as one with the line defect are calculated to show how these defects impact the collective mechanical properties, as presented in Figure 3b. It can be easily observed that the more uniformly distributed the stress is over the graphene sheet, the more superior the mechanical properties are in terms of ultimate stress and strain. It is noteworthy that the ultimate strength and strain of the graphene with the line defect are 89% and 85% of the pristine graphene, suggesting a rather low mechanical degradation. The white line in Figure 2b represents square-shaped defects, indicating that the larger the defect, the weaker the mechanical strength. which can be also interpreted by the governance of the $L_{\perp}$ effect.

Comparing the above defective graphene sheets with a rectangular defect in Figure 3 to one with a circular defect in Figure 1c, g, it can be seen that although they both produce high- and low-stress regions and induce the out-of-plane/in-plane behavior, the difference can be spotted on how the defect shapes these influenced regions. For example, the high-stress regions of graphene with a rectangular defect are well distributed along the defect edges and the low-stress regions are formed in a spread out fashion. A circular defect produces high-stress regions emitting from a part of the defect rim while having more localized low-stress regions. In addition, the displacement behavior is more profound when a rectangular defect is present other than a circular defect. These differences subsequently give rise to different collective mechanical properties of the defective graphene sheets. To shed light on the source of these differences, it is crucial to investigate not only the defect size but also the defect shape.

Having discussed the influence of $(L_{\|},L_{\perp})$ on the mechanical properties of defective graphene sheets, the possible impact caused by different defect shapes is investigated where the parameter pair $(L_{\|},L_{\perp})$ is set as fixed. To this end, a square-shaped defect, a circular defect, and a diamond-shaped defect with $L_{\perp} = L_{\|} = 0.3L$ are inspected. The original shapes, stress fields, distributions of out-of-plane and in-plane displacement magnitude, and stress−strain curves are shown in Figure 4a−c, d−f, g−i, j−l, and m, respectively. Stress fields of the above defective graphene sheets reveal a significant shape-related difference. Among these defects, the square-shaped defect produces the most even stress field where high stress is uniformly distributed long two edges parallel to the stretch, while the diamond-shaped defect is featured by an outstanding stress concentration at the upper and lower vertices. The effect

https://dx.doi.org/10.1021/acs.jpcc.9b11027
J. Phys. Chem. C XXXX, XXX, XXX−XXX

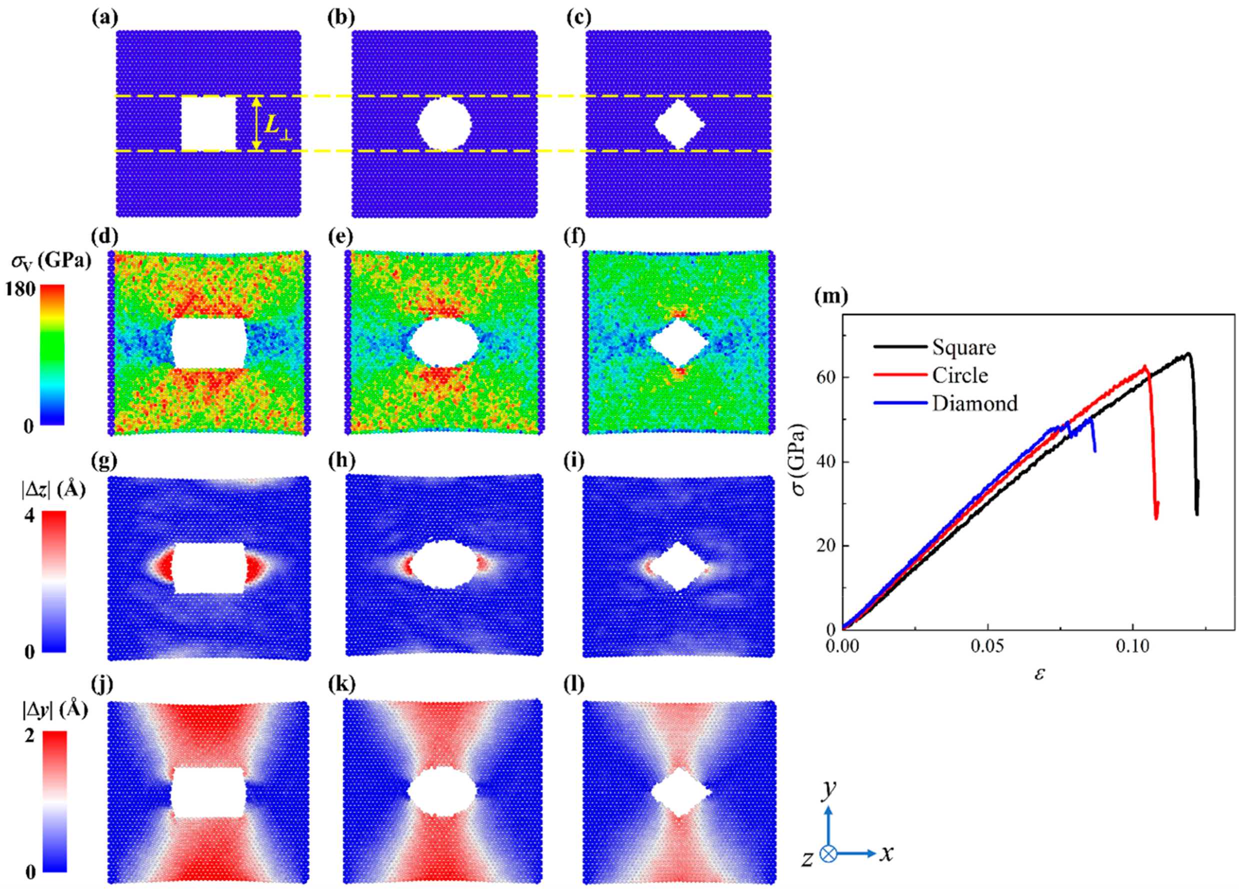

Figure 4. Influence of defect shape on the mechanical properties of graphene sheets. (a−c) Initial shapes, (d−f) stress fields, distributions of (g−i) out-of-plane and (j−l) in-plane displacement magnitude, and (m) stress−strain curves of square-shaped, circular, and diamond-shaped defects.

of the circular defect lies in between the square-shaped defect and the diamond-shaped defect. Stress−strain curves of these three defective graphene sheets in Figure 4m show that the graphene sheet with a square defect possesses the best mechanical properties while the graphene sheet with the diamond defect is the weakest. Therefore, similarly, the square defect renders the most profound out-of-plane and in-plane behavior while the diamond defect does the least, as shown in Figure 4g−l. It is interesting that although the square-shaped defect requires the removal of the most number of atoms, it yields the highest failure stress and strain. This implies that the defect shape is a new factor to consider and opens up possibilities of defect design. From Figure 4, two major observations can be readily made: (1) High stress is concentrated at the farthest reach of the defect geometry transverse to the stretching direction, by which high-stress regions can be straightforwardly determined by inspection. (2) Dichotomizing points on the defect rim of out-of-plane-intense and in-plane-intense regions also dichotomize the low-stress and above-moderate stress regions, of which the locations are a function of the defect curve.

An analytical framework is developed as follows to pinpoint the dichotomizing points of a general plane curve $\gamma(s) = (x(s),y(s))$. Slopes of the tangent and the normal lines at a point $(x(s_0),y(s_0))$ are $k(s_0) = \mathrm{d}y/\mathrm{d}x|_{s=s_0}$ and $n(s_0) = -\mathrm{d}x/\mathrm{d}y|_{s=s_0}$. Projecting the external loading onto the two directions, we obtain the tangential force $F_t(s_0)$ and the normal force $F_n(s_0)$. It can be assumed that the tangential force raises stress by the in-plane stretching while the normal force does not contribute to stress at the examined point on the defect rim (because there is no atom inside the defect to balance the normal component). These two effects counteract each other. The dominance of the tangential force over the normal force gives rise to a high stress level, while the dominance of the normal force features a low stress. If the tangential force and the normal force are equal at certain points on the defect rim, these points dichotomize the high and low stress regions. This happens where the angle between the tangential and external tensile loading is $\pi/4$. Specifically, in this study where the stretch is along the x-axis, the requirement is simplified to the following: high stress: $|k| < 1$; low stress: $|k| > 1$; critical slope: $|k_{cr}| = 1$. In fact, calculating the slope of a tangent line task for a given plane curve $\boldsymbol{\gamma}(s) = (x(s),y(s))$ is a relatively easy task. The effectiveness of the above methods is tested by some examples.

(1) Rectangular Defects. The defect rim of a rectangular defect has slopes of either $k = 0$ (edges parallel to the loading) or $k = \infty$ (edges perpendicular to the loading). Upon stretching, edges originally parallel to the loading remain parallel, emanating high stress regions. Edges perpendicular to the stretch swell by a small amount, where it is rational to assume that no point on the edges has a slope with an absolute value smaller than 1, hence initiating low stress regions. Dichotomizing points lie right on the four vertices. The above reasoning is confirmed by various results in Figure 3.

(2) Diamond-Shaped Defects. Edges of diamond-shaped defects possess slopes of an identical absolute value $|k_d|$. It is envisioned that if $|k_d| < 1$, all edges contribute to high stress

https://dx.doi.org/10.1021/acs.jpcc.9b11027
J. Phys. Chem. C XXXX, XXX, XXX−XXX

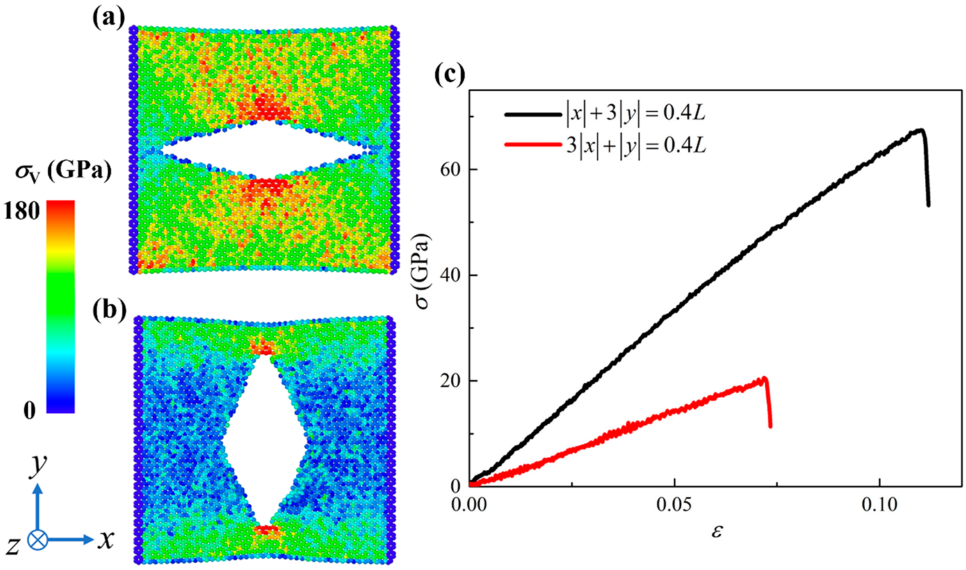

Figure 5. Simulation results of graphene sheets with a centered diamond-shaped defect. Stress distributions of graphene sheets with diamond-shaped defects parametrized by (a) $|x| + 3|y| = 0.4L$ and (b) $3|x| + |y| = 0.4L$. (c) Stress−strain curves of above two defective graphene sheets.

while low stress only appears at the vicinity of vertices on the x-axis. If $|k_d| > 1$, all edges contribute to low stress while high stress only appears at the vicinity of vertices on the y-axis (regions of stress concentration). The above hypothesis is tested by simulating two graphene sheets with diamond-shaped defects $|x| + 3|y| = 0.4L$ and $3|x| + |y| = 0.4L$, respectively. Edges of the former diamond have a slope of $k_d = \pm 1/3$, while those for the latter have a slope of $k = \pm 3$. Simulation results are shown in Figure 5, which confirm our hypothesis.

(3) Defects with a Curved Rim. Defects with a curved rim distinguish themselves from previously discussed rectangular and diamond-shaped defects in that the curvature of the rim renders the continuous variation of tangential direction. Therefore, the dichotomizing points are to be determined by solving $k(s) = dy/dx = \pm 1$. Circular, elliptical, quadratic polynomial-shaped, and sine-shaped defects are utilized to test our method, of which the curve equations and derived dichotomizing points are summarized in Table S1 in Supporting Information. The predictions are tested by an example of each of the four classes. They are (a) $[x/(1 + \varepsilon)]^2 + y^2 = (0.15L)^2$, (b) $[x/(1 + \varepsilon)]^2/(0.2L)^2 + y^2/(0.1L)^2 = 1$, (c) $y = (4.8/L)\{(0.25L)^2 - [x/(1 + \varepsilon)]^2\}$, and (d) $y = 0.2L \cos\{(2\pi/L)[x/(1 + \varepsilon)]\}$, where ε is chosen as the strain immediate to the onset of fracture (0.101, 0.129, 0.0951, and 0.0932, respectively, for the four cases above). Predicted results are compared against the stress fields from MD simulations, as shown in Figure 6, where predicted dichotomizing points are marked by red arrows. A good agreement between predictions and simulation results is reached, showing the validity of the method to address defects of all shapes.

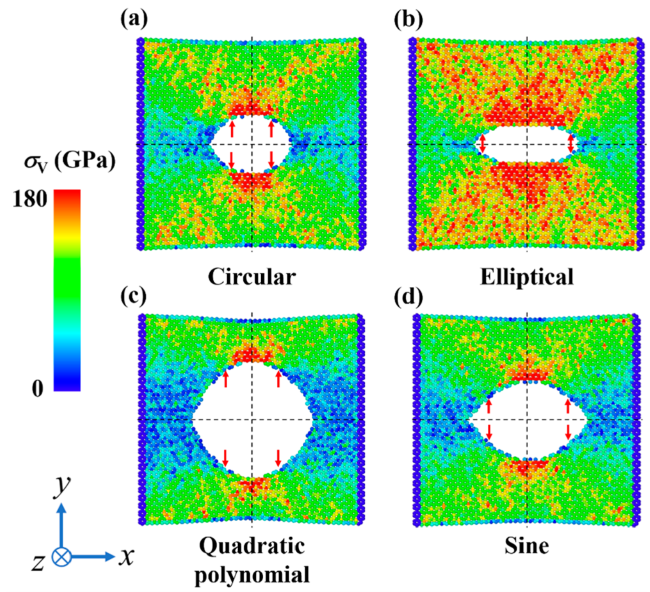

Figure 6. Comparisons between predicted dichotomizing points and simulation results of graphene sheets with a (a) circular defect, (b) elliptical defect, (c) quadratic polynomial-shaped defect, and (d) sine-shaped defect.

Having qualitatively and quantitatively studied the influence of a single defect, scenarios where multiple defects are present can be readily discussed. The above results of a single defect show that high-stress regions are located at the farthest ends of the defect transverse to the stretch. When multiple defects are present, this conclusion still holds by applying the strategy of defect grouping. When defects have overlaps transverse to the stretch, they can be viewed as a group and the farthest ends of the defect group localize high-stress regions. In Figure 7a, stress fields of graphene sheets with two rectangular defects with overlaps transverse to the stretch are illustrated, one with rectangular defects of different sizes ((0.1L, 0.4L) and (0.1L, 0.6L)) and the other with two identical defects (both (0.1L, 0.4L)). The geometric centers of two defects are aligned on the center line parallel to the stretch and trisection of the graphene sheets. As can be seen, high-stress regions reside at the farthest ends of the defect group transverse to the stretch. For the graphene sheet with defects of different sizes, the ends of the smaller defect do not concentrate stress, while both ends of the larger defect do. For the graphene sheet with identical defects, both defects concentrate stress at their two ends; thus, in this case, high-stress regions are significantly larger, an indicator of a more uniform stress distribution. The same principle applies to circular defects, as is shown in Figure 7b, where the

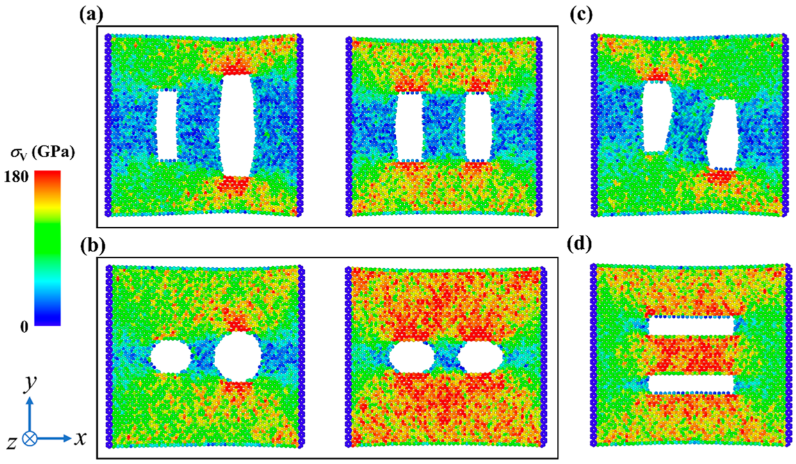

Figure 7. Stress fields of graphene sheets with two defects. Graphene sheets with two (a) rectangular and (b) circular defects aligned on the center line parallel to the stretch. (c) Graphene sheet with two identical rectangular defects but not aligned on the center line parallel to the stretch. (d) Graphene sheet with two identical rectangular defects with no overlap transverse to the stretch.

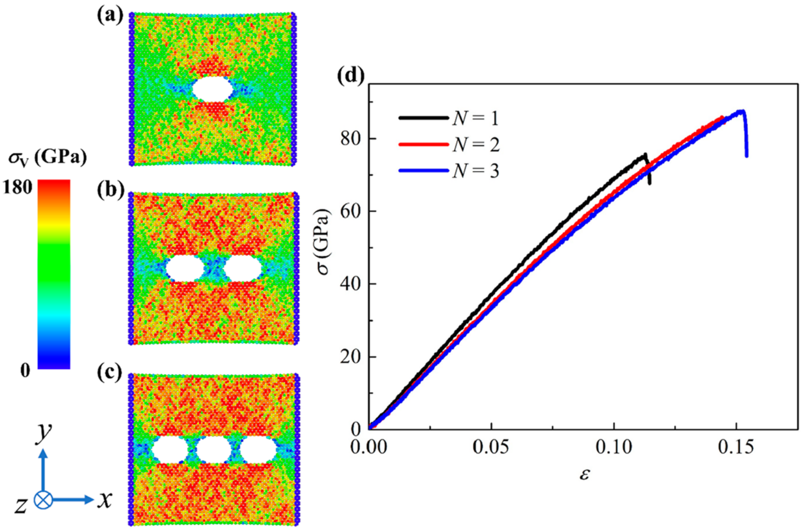

Figure 8. Simulation results of graphene sheets with N circular defects aligned in the stretching direction. Stress distributions for (a) $N = 1$, (b) $N = 2$, and (c) $N = 3$. (d) Stress−strain curves for $N = 1$−3.

diameters are 0.2L and 0.3L for the graphene sheets with circular defects of different sizes and 0.2L for two identical defects. Also, by this principle, it is possible that only one end of a defect localizes high stress instead of both ends or no end. To showcase this, a graphene sheet with two identical defects (both (0.1L, 0.4L)) not aligned on the center line are simulated. Each defect has an offset of 0.05L from the centerline but in the opposite directions. The stress field in Figure 7c shows that high-stress regions are located at the two farthest ends of the defect group, which in this case takes on one end from each of the two defects. When multiple defects have no overlaps transverse to the stretch and do not form a defect group, each defect affects the stress field independently. Figure 7d presents the case of two identical rectangular defects (both (0.1L, 0.4L)) having no overlaps transverse to the stretch. As can be seen, both defects produce two high-stress and two low-stress regions. However, it is noteworthy that, due to the potential overlaps of high-stress regions by individual defects, some parts of the stress field can be double-strengthened, such as in between the two defects in Figure 7d. The stress−strain curves of defective graphene sheets are provided in Figure S2 in the Supporting Information.

From Figure 7b, it can be seen that a relatively small modification of defects can make a profound difference to the stress field, where the stress field is much more uniform when two identical defects are present. This inspires the optimization of the stress field by placing defects in the right locations. As a preliminary exploration, mechanical properties of graphene sheets with N identical circular defects aligned on the centerline parallel to the stretch are studied. The defect diameter is 0.2L and N = 1−3. Stress fields of graphene sheets with one, two, and three circular defects are shown in Figures 8a−c, respectively. It can be observed that, as the number of defects increases, the stress field becomes more and more uniform. Corresponding stress−strain curves of these graphene sheets are compared in Figure 8d. It is shown that the ultimate strength and strain can be stably enhanced with the increasing defect number even if more and more atoms are removed from the graphene sheet. It is worth mentioning that what dominates this strengthening effect is not a particular parameter such as defect size, shape, number, and alignment.

https://dx.doi.org/10.1021/acs.jpcc.9b11027
J. Phys. Chem. C XXXX, XXX, XXX−XXX

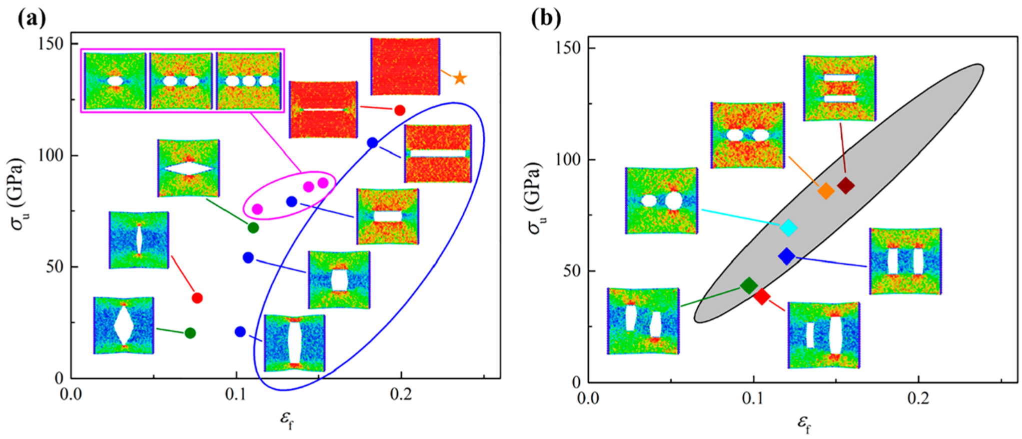

Figure 9. $\sigma_u-\varepsilon_f$ plots summarizing mechanical properties of all the defects studied. Graphene sheets with (a) a single defect and (b) multiple defects. The gray area in (b) represents the distribution of data points in (a).

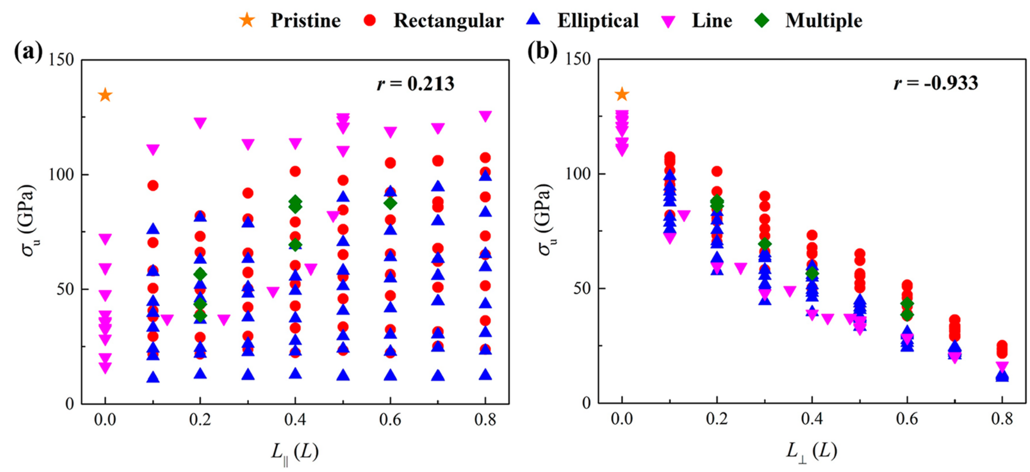

Figure 10. Influences of $L_\parallel$ and $L_\perp$ on the ultimate strength σ_u of the defective graphene sheet. σ_u as a function of (a) $L_\parallel$ and (b) $L_\perp$. Data points of elliptical and line defects are from refs 34 and 37.

Rather, it is how a more uniform stress field can be created by defect design. Adding identical defects parallel to the stretch is one way but not the only way to create a more uniform stress field. Also, this application has illustrated the potential of enhancing the mechanical properties of graphene by optimizing defects. This result is found to be consistent with classical mechanics. For a plate with a row of collinear holes, it is shown by boundary element methods that the maximum circumferential stress along the central hole decreases with an increasing number of holes.[39] This indicates a reduced stress concentration around stress raisers and an enhanced collective mechanical property, which is observed in our results. In addition, the results of classical mechanics also show that as the number of holes increases, the decrease of the maximum stress slows down and the stress approaches an asymptotic solution.[40] The same tendency is shown in our simulation with an increasing number of collinear circular defects. Several important conclusions are the same across a broad range materials, scales, and numerical methods. Hence, it is envisioned that this enhancing effect can be extended to other 2D materials.

3. DISCUSSION

Having studied a broad variety of defects as well as their combinations featured by a wide spectrum of mechanical properties, up to this point, it is necessary to summarize all the results and interesting to check if these different defect configurations share any underlying common ground. The mechanical properties of all defective graphene sheets in the present study are summarized in $\sigma_u-\varepsilon_f$ plots in Figure 9, where ε_f denotes the failure strain. Figure 9a presents the results of graphene sheets with a single defect. Results of mechanical enhancement by increasing defect number in Figure 8 are also included to illustrate the evolution path starting from a single circular defect to multiple identical collinear defects. The data point of the pristine graphene is also provided in Figure 9a for reference, as is marked with the star symbol. As can be seen, despite the difference in defect geometry, all results lie within a narrow-banded region, with no exception of the pristine graphene sheet. This suggests that the variation of defect geometry, though resulting in drastically different mechanical properties, in general preserves the proportionality of ultimate strength and failure strain. Graphene sheets with multiple defects are summarized in Figure 9b. The gray region represents the banded region in Figure 9a which embodies the proportionality. As can be seen, results of various configurations of multiple defects still lie within the banded region, suggesting that the proportionality is one of the underlying common grounds of various defective graphene sheets (including the pristine graphene sheet).

https://dx.doi.org/10.1021/acs.jpcc.9b11027
J. Phys. Chem. C XXXX, XXX, XXX−XXX

Another way of a summary is to plot mechanical properties such as ultimate strength against parameters, which can help shed light on the relative significance of system parameters by examining the relevancy and distribution pattern. Here, σ_u as a function of $L_{\parallel}$ and $L_{\perp}$ for all defect shapes and configurations in the present paper as well as in our previous work[34,37] is investigated, as is summarized in Figure 10. In Figure 10a, no outstanding correlation between $L_{\parallel}$ and σ_u is exhibited and Pearson's correlation coefficient r is calculated to be 0.213, indicating that $L_{\parallel}$ may not be a governing factor of mechanical properties of defective graphene sheets. Contrarily, the banded distribution in Figure 10b shows a strong correlation between $L_{\perp}$ and σ_u, with an r value of −0.933. Therefore, $L_{\perp}$ is a much more dominant parameter than $L_{\parallel}$. In addition, Figure 10b is able to give a strong indication on the relative significance of size effect and shape effect, where the latter can be reflected by the width of the banded distribution under a certain $L_{\perp}$ value. It is noteworthy that, at a given $L_{\perp}$, rectangular defects possess higher σ_u than elliptical defects.

4. CONCLUSIONS

In this paper, stress field characteristics of defective graphene sheet subject to unidirectional in-plane stretch are studied via MD simulation. It is shown that stress distribution is strongly dependent on defect properties, which ultimately impacts collective mechanical properties such as strength and ductility. The out-of-plane degree of freedom can be released by the introduction of defects and the relationship between stress distribution and displacement patterns are revealed. The effect of defect geometry can be decoupled by studying defect size and shape, where the former determines the area shielded from increasing stress and consequently produces low-stress regions, while the latter determines local stress concentration and governs stress distribution along the defect rim. An analytical approach is developed to pinpoint the dichotomizing points on the defect rim, which shows good agreement with the results of MD simulations. The strategy of defect grouping is proposed to analyze the stress field when multiple defects are present in the graphene sheet. Knowing the relation between defect properties and stress distribution characteristics, the optimization of mechanical properties can be achieved by rational defect design. In addition, it is shown that even though the mechanical properties of defective graphene sheets vary with different defect geometry, the proportionality of ultimate strength and failure strain is in general preserved. Finally, the relative significance of the system parameters is discussed. This paper has systematically discussed the influence of defects on the stress distribution in graphene sheets, which opens up the tuning approach of the mechanical properties of graphene as well as other 2D materials via defect engineering. A major contribution of the present work is the incorporation of variable defect presentations into the feature of the stress field only, which enables us to evaluate the collective properties and pinpoint regions prone to fracture of defective graphene *a priori*. Stress field characteristics of defective graphene sheets under more complex loading conditions such as bending, twisting, and impact loading will be covered in the future work.

■ ASSOCIATED CONTENT

Supporting Information

The Supporting Information is available free of charge at https://pubs.acs.org/doi/10.1021/acs.jpcc.9b11027.

Settings of MD simulation; calculation method of stress; discussion of strain rate effect; analytical results of dichotomizing points; stress−strain curves of graphene sheets with multiple defects (PDF)

■ AUTHOR INFORMATION

Corresponding Author

Grace X. Gu − *Department of Mechanical Engineering, University of California, Berkeley, California 94720, United States*; orcid.org/0000-0001-7118-3228; Phone: 510-643-4996; Email: ggu@berkeley.edu

Author

Bowen Zheng − *Department of Mechanical Engineering, University of California, Berkeley, California 94720, United States*

Complete contact information is available at: https://pubs.acs.org/10.1021/acs.jpcc.9b11027

Notes

The authors declare no competing financial interest.

■ ACKNOWLEDGMENTS

The authors acknowledge support from the Extreme Science and Engineering Discovery Environment (XSEDE) at the Pittsburgh Supercomputing Center (PSC) through allocation TG-DMR180085, by National Science Foundation Grant Number ACI-1548562. Additionally, the authors acknowledge support from an NVIDIA GPU Seed Grant and the Savio computational cluster resource provided by the Berkeley Research Computing program.

■ REFERENCES

(1) Lee, C.; Wei, X.; Kysar, J. W.; Hone, J. Measurement of the Elastic Properties and Intrinsic Strength of Monolayer Graphene. *Science* **2008**, *321*, 385−388.

(2) Young, R. J.; Kinloch, I. A.; Gong, L.; Novoselov, K. S. The Mechanics of Graphene Nanocomposites: A Review. *Compos. Sci. Technol.* **2012**, *72*, 1459−1476.

(3) Wan, S.; Peng, J.; Li, Y.; Hu, H.; Jiang, L.; Cheng, Q. Use of Synergistic Interactions to Fabricate Strong, Tough, and Conductive Artificial Nacre Based on Graphene Oxide and Chitosan. *ACS Nano* **2015**, *9*, 9830−9836.

(4) Chen, C.-T.; Martin-Martinez, F. J.; Ling, S.; Qin, Z.; Buehler, M. J. Nacre-Inspired Design of Graphene Oxide−Polydopamine Nanocomposites for Enhanced Mechanical Properties and Multi-Functionalities. *Nano Futures* **2017**, *1*, 011003.

(5) Xu, Z.; et al. Ultrastiff and Strong Graphene Fibers Via Full-Scale Synergetic Defect Engineering. *Adv. Mater.* **2016**, *28*, 6449−6456.

(6) Papageorgiou, D. G.; Kinloch, I. A.; Young, R. J. Mechanical Properties of Graphene and Graphene-Based Nanocomposites. *Prog. Mater. Sci.* **2017**, *90*, 75−127.

(7) Chen, C. T.; Gu, G. X. Effect of Constituent Materials on Composite Performance: Exploring Design Strategies Via Machine Learning. *Adv. Theory Simul.* **2019**, *2*, 1900056.

(8) Martin-Olmos, C.; Rasool, H. I.; Weiller, B. H.; Gimzewski, J. K. Graphene Mems: Afm Probe Performance Improvement. *ACS Nano* **2013**, *7*, 4164−4170.

(9) Bunch, J. S.; van der Zande, A. M.; Verbridge, S. S.; Frank, I. W.; Tanenbaum, D. M.; Parpia, J. M.; Craighead, H. G.; McEuen, P. L. Electromechanical Resonators from Graphene Sheets. *Science* **2007**, *315*, 490−493.

(10) Zhu, J.; Childress, A. S.; Karakaya, M.; Dandeliya, S.; Srivastava, A.; Lin, Y.; Rao, A. M.; Podila, R. Defect-Engineered Graphene for

High-Energy- and High-Power-Density Supercapacitor Devices. *Adv. Mater.* **2016**, *28*, 7185−7192.
(11) Wang, Y.; Shi, Z.; Huang, Y.; Ma, Y.; Wang, C.; Chen, M.; Chen, Y. Supercapacitor Devices Based on Graphene Materials. *J. Phys. Chem. C* **2009**, *113*, 13103−13107.
(12) Stampfer, C.; Schurtenberger, E.; Molitor, F.; Güttinger, J.; Ihn, T.; Ensslin, K. Tunable Graphene Single Electron Transistor. *Nano Lett.* **2008**, *8*, 2378−2383.
(13) Lin, Y.-M.; Jenkins, K. A.; Valdes-Garcia, A.; Small, J. P.; Farmer, D. B.; Avouris, P. Operation of Graphene Transistors at Gigahertz Frequencies. *Nano Lett.* **2009**, *9*, 422−426.
(14) Saffarzadeh, A.; Farghadan, R. A Spin-Filter Device Based on Armchair Graphene Nanoribbons. *Appl. Phys. Lett.* **2011**, *98*, 023106.
(15) Green, A. A.; Hersam, M. C. Solution Phase Production of Graphene with Controlled Thickness Via Density Differentiation. *Nano Lett.* **2009**, *9*, 4031−4036.
(16) Yi, M.; Shen, Z. A Review on Mechanical Exfoliation for the Scalable Production of Graphene. *J. Mater. Chem. A* **2015**, *3*, 11700−11715.
(17) Chen, Z.; Ren, W.; Gao, L.; Liu, B.; Pei, S.; Cheng, H.-M. Three-Dimensional Flexible and Conductive Interconnected Graphene Networks Grown by Chemical Vapour Deposition. *Nat. Mater.* **2011**, *10*, 424.
(18) Mattevi, C.; Kim, H.; Chhowalla, M. A Review of Chemical Vapour Deposition of Graphene on Copper. *J. Mater. Chem.* **2011**, *21*, 3324−3334.
(19) Berger, C.; et al. Ultrathin Epitaxial Graphite: 2d Electron Gas Properties and a Route toward Graphene-Based Nanoelectronics. *J. Phys. Chem. B* **2004**, *108*, 19912−19916.
(20) Berger, C.; et al. Electronic Confinement and Coherence in Patterned Epitaxial Graphene. *Science* **2006**, *312*, 1191−1196.
(21) Tang, C.; Wang, B.; Wang, H.-F.; Zhang, Q. Defect Engineering toward Atomic Co−Nx−C in Hierarchical Graphene for Rechargeable Flexible Solid Zn-Air Batteries. *Adv. Mater.* **2017**, *29*, 1703185.
(22) Wang, Y.; Chen, S.; Ruan, X. Tunable Thermal Rectification in Graphene Nanoribbons through Defect Engineering: A Molecular Dynamics Study. *Appl. Phys. Lett.* **2012**, *100*, 163101.
(23) Lakshmi, S.; Roche, S.; Cuniberti, G. Spin-Valve Effect in Zigzag Graphene Nanoribbons by Defect Engineering. *Phys. Rev. B: Condens. Matter Mater. Phys.* **2009**, *80*, 193404.
(24) Tang, C.; Zhang, Q. Nanocarbon for Oxygen Reduction Electrocatalysis: Dopants, Edges, and Defects. *Adv. Mater.* **2017**, *29*, 1604103.
(25) Anno, Y.; Imakita, Y.; Takei, K.; Akita, S.; Arie, T. Enhancement of Graphene Thermoelectric Performance through Defect Engineering. *2D Mater.* **2017**, *4*, 025019.
(26) Blees, M. K.; et al. Graphene Kirigami. *Nature* **2015**, *524*, 204.
(27) Shyu, T. C.; Damasceno, P. F.; Dodd, P. M.; Lamoureux, A.; Xu, L.; Shlian, M.; Shtein, M.; Glotzer, S. C.; Kotov, N. A. A Kirigami Approach to Engineering Elasticity in Nanocomposites through Patterned Defects. *Nat. Mater.* **2015**, *14*, 785.
(28) Wei, N.; Chen, Y.; Cai, K.; Zhao, J.; Wang, H.-Q.; Zheng, J.-C. Thermal Conductivity of Graphene Kirigami: Ultralow and Strain Robustness. *Carbon* **2016**, *104*, 203−213.
(29) Bai, J.; Zhong, X.; Jiang, S.; Huang, Y.; Duan, X. Graphene Nanomesh. *Nat. Nanotechnol.* **2010**, *5*, 190.
(30) Jiang, L.; Fan, Z. Design of Advanced Porous Graphene Materials: From Graphene Nanomesh to 3d Architectures. *Nanoscale* **2014**, *6*, 1922−1945.
(31) Zhu, S.; Huang, Y.; Li, T. Extremely Compliant and Highly Stretchable Patterned Graphene. *Appl. Phys. Lett.* **2014**, *104*, 173103.
(32) Hao, F.; Fang, D.; Xu, Z. Mechanical and Thermal Transport Properties of Graphene with Defects. *Appl. Phys. Lett.* **2011**, *99*, 041901.
(33) Wang, M. C.; Yan, C.; Ma, L.; Hu, N.; Chen, M. W. Effect of Defects on Fracture Strength of Graphene Sheets. *Comput. Mater. Sci.* **2012**, *54*, 236−239.
(34) Zheng, B.; Gu, G. Recovery from Mechanical Degradation of Graphene by Defect Enlargement. *Nanotechnology* **2020**, *31*, 085707.
(35) Eshkalak, K. E.; Sadeghzadeh, S.; Jalaly, M. Studying the Effects of Longitudinal and Transverse Defects on the Failure of Hybrid Graphene-Boron Nitride Sheets: A Molecular Dynamics Simulation. *Phys. E* **2018**, *104*, 71−81.
(36) Eshkalak, K. E.; Sadeghzadeh, S.; Jalaly, M. Mechanical Properties of Defective Hybrid Graphene-Boron Nitride Nanosheets: A Molecular Dynamics Study. *Comput. Mater. Sci.* **2018**, *149*, 170−181.
(37) Zheng, B.; Gu, G. X. Tuning Graphene Mechanical Anisotropy Via Defect Engineering. *Carbon* **2019**, *155*, 697−705.
(38) Qi, Z.; Campbell, D. K.; Park, H. S. Atomistic Simulations of Tension-Induced Large Deformation and Stretchability in Graphene Kirigami. *Phys. Rev. B: Condens. Matter Mater. Phys.* **2014**, *90*, 245437.
(39) Wang, J.; Crouch, S. L.; Mogilevskaya, S. G. A Complex Boundary Integral Method for Multiple Circular Holes in an Infinite Plane. *Eng. Anal. Bound. Elem.* **2003**, *27*, 789−802.
(40) Horii, H.; Nemat-Nasser, S. Elastic Fields of Interacting Inhomogeneities. *Int. J. Solids Struct.* **1985**, *21*, 731−745.